Neuroradiology (1992) 35: 1–9

Diagnostic Neuroradiology

Neuro radiology

Cerebrospinal fluid flow

I. Physiology of cardiac-related pulsation

G. Schroth and U. Klose

Department of Neuroradiology, University of Tübingen, Federal Republic of Germany

Received: 5 November 1990

Summary. Cardiac-related motion of the cerebrospinal fluid (CSF) was investigated by analysis of the velocity-dependent phase of CSF protons and flow-dependent signal enhancement in magnitude images using ECG-gated FLASH sequences. In the cerebral aqueduct, CSF flow from the third to the fourth ventricle begins 200 ms after the R-wave of the ECG and simulates an arterial pulse wave pattern. It lasts about 60 % of the cardiac cycle and is followed by backflow from the fourth to the third ventricle, which is slower and shorter. In the spinal canal, oscillating caudad motion precedes flow from the third to the fourth ventricle by about 50–100 ms and is superimposed on a bulk flow, which moves simultaneously in opposite directions in separate subarachnoid channels; it is directed mainly caudally in the anterior cervical subarachnoid space.

Key words: Magnetic resonance imaging – Cerebrospinal fluid flow

Knowledge of the production, distribution, and absorption of cerebrospinal fluid (CSF) has gradually increased since the introduction of radionuclide scanning [1, 2] and X-ray contrast cinecisternography and cineventriculography [3, 4]. However, understanding of CSF flow is still incomplete, and hampered by the fact that lumbar puncture of the closed system of the CSF spaces may disturb physiological movements. Moreover, in the earlier investigations it was necessary to replace incompressible CSF with highly compressible air or oily myelographic contrast medium with a high specific gravity, or both [3–5].

With magnetic resonance imaging (MRI), normal and pathological CSF movements can be visualized and quantified noninvasively [6–10] and mapping of flow patterns can be achieved in a variety of pathological conditions.

Methods

Thirty normal volunteers, 18–40 years old, were investigated using a 1.5 T unit. Cardiac gating was performed with a commercially available device, which could also be used for flow-phantom measurements. Following the R wave of the ECG, a slice at a given anatomical position was excited 20 times, beginning with every second or third R wave (Fig. 1). Using FLASH sequences [11] with a repetition time of 75 ms and an echo time of 10 ms, one measurement takes 1.5 s and lasts longer than one cardiac cycle (Fig. 1). Thus, all cardiac-related motion perpendicular to the excited slice during one cardiac cycle can be detected even in bradycardia, and the periodic repetition of the CSF pulsation is directly demonstrated on the plot of signal intensity [9]. When higher time resolution was required, repetition time was decreased to 30 ms, acknowledging the disadvantage of a measurement time shorter than one cardiac cycle.

Due to the cardiac gating, the repetition time for the first image of the series is prolonged (Fig. 1) resulting in increased signal intensity. This effect has to be taken into consideration for quantitative flow measurement: the overall signal increase if the image has to be subtracted, or the signal intensity during the second cardiac cycle (Fig. 1) must be studied.

In order to obtain high contrast between flowing and stationary structures, a large flip angle (90°) was applied [9]. A striking feature of these FLASH images is the high signal from flowing media, especially when motion is perpendicular to the image plane. This signal enhancement is due to wash-in of fully relaxed spins between radio frequency pulses, whereas the signal intensity of stationary structures is decreased by saturation effects during the

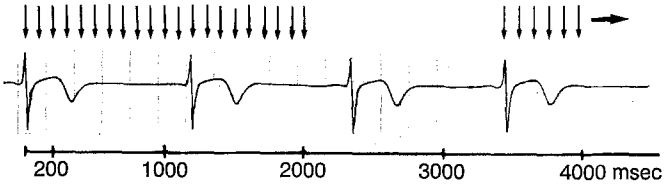

Fig. 1. ECG-gated FLASH sequence for detection of signal changes in the cardiac cycle. The same slice is exited 20 times perpendicular to the expected flow, starting every second or third R wave of the ECG

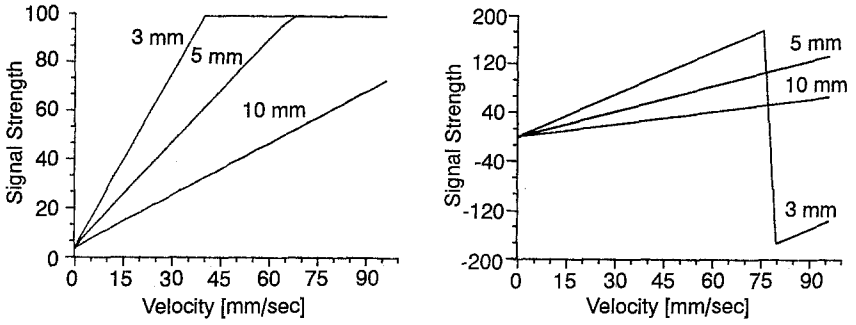

Fig. 2. Computer simulation of signal intensity and phase, plotted as a function of increasing flow for slices 3.5 and 10 mm thick (FLASH, TR = 75 ms, TE = 10 ms, flip angle: 90°)

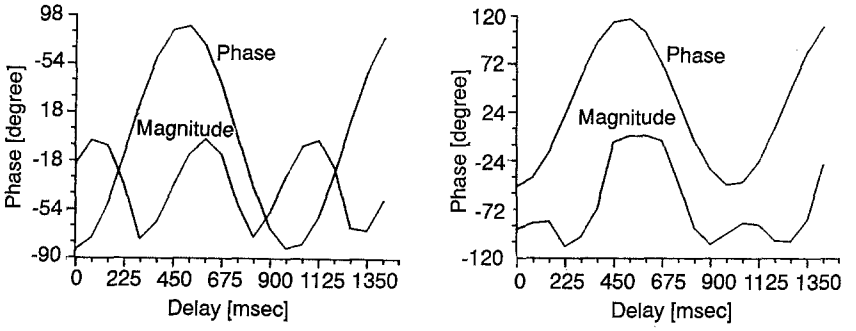

Fig. 3. Computer-simulated changes in signal strength and phase of an oscillating motion plotted together in one diagram. Signal increase follows the increase and decrease of phase with a typical time delay *(left). Right:* Oscillating motion is superimposed on an additional directed flow (bulk flow: 3 mm/s, maximum speed of the oscillating flow: 5 mm/s; FLASH, TR = 75 ms, TE = 10 ms, slice thickness = 5 mm): signal intensity is increased when the oscillating flow and the bulk flow move in the same direction and decreased when they are in opposite directions

course of the 256 excitations applied in order to form a 256 × 256 matrix image.

Movement of CSF was calculated by flow-induced signal enhancement on magnitude images and by registration of the flow-dependent phase of the protons on phase images. Comparative analysis of both signal strength and phase proved necessary for correct interpretation of the complex flow-pattern of the CSF. Computer-simulated calculations and phantom measurements demonstrated that the velocity-dependent increases of signal intensity and phase were simultaneous in laminar plug flow (Fig. 2). With sinusoidal oscillating flow, however, there was a delay between phase and signal intensity (Fig. 3): signal increase followed the change of phase with a time delay dependent upon the amplitude and velocity of the pulsation. When the pulsatile flow changed its direction, protons which had just been saturated entered the excited slice in the opposite direction. This resulted in delayed signal increase in oscillating flow compared with the real flow acceleration shown by the phase diagram. By comparing both signal intensity – with its "memory of ancient movement" – and phase, optimal interpretation of CSF flow was possible.

To simulate the complex flow pattern of an oscillating motion superimposed on an additional directional flow, as expected in the spinal canal [9], a special flow phantom was developed (Fig. 4). Phantom measurements and computer-simulated calculations confirmed high signal increase when the oscillating flow and bulk flow moved in the same direction. However, the signal was decreased when the oscillating and directed flows were opposed (Fig. 3).

Additional application of saturation pulses above or below the slices examined [9] enables determination of the direction of CSF flow (Fig. 10). By varying slice thickness and the distance of the saturation slice from the slice examined, flow velocities and the amplitude of the oscillating flow component can be calculated.

Results

Using paraxial slices, CSF flow was measured perpendicular to the expected flow within the cerebral aqueduct, the foramen of Monro, and the cervical spinal canal. In each case, signal intensity and phase of the adjacent brain were measured as additional internal standards.

Serial ECG-gated FLASH images through the inferior colliculus clearly demonstrate the oscillating CSF flow in the cerebral aqueduct on magnitude and phase images

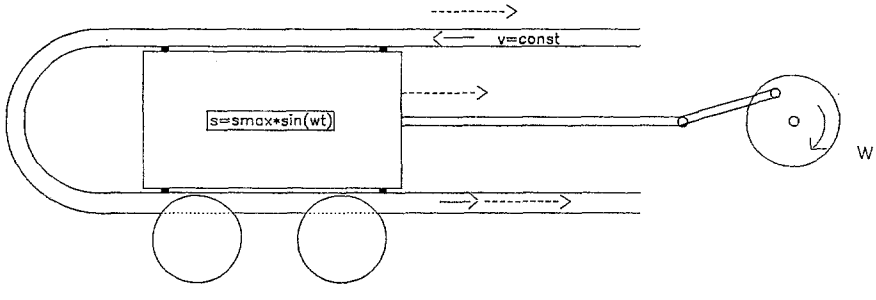

Fig. 4. Flow phantom: concentric tubes perfused with water are fixed to a wagon moving backwards and forwards through the magnetic field. By varying the amplitude and frequency of the wagon's motion and the flow inside the tubes any combination of directional flow and superimposed oscillating motion can be achieved

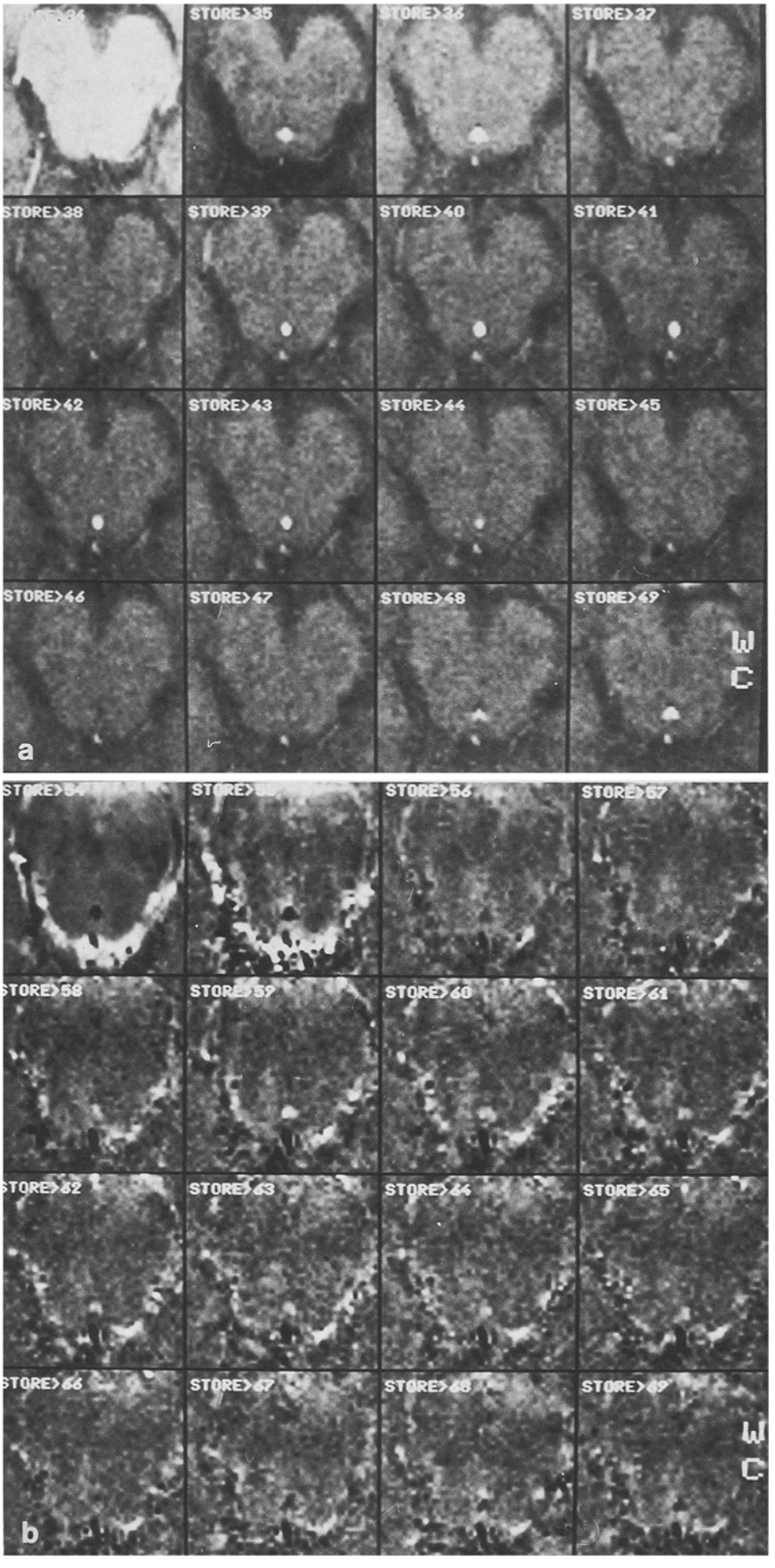

Fig. 5 a, b. Serial ECG-gated FLASH images through the inferior colliculus of the tectum mesencephalic. The magnitude images (**a**) demonstrate oscillating increase and decrease of signal intensity in the cerebral aqueduct, whereas the signal in the superior cerebellar vein remains high during the whole cardiac cycle. In the corresponding phase images (**b**) flow downwards is encoded as decrease, upwards as increase of signal intensity

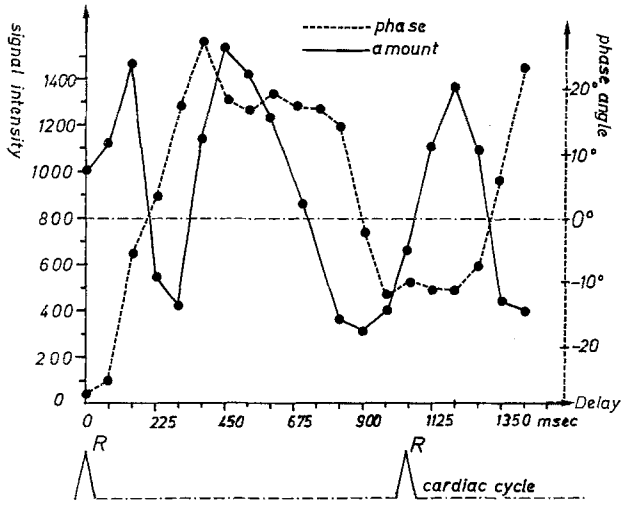

Fig. 6. Signal intensity and phase as a function of R wave delay of four central voxels in the cerebral aqueduct are presented in one diagram to confirm the time delay between phase and signal strength

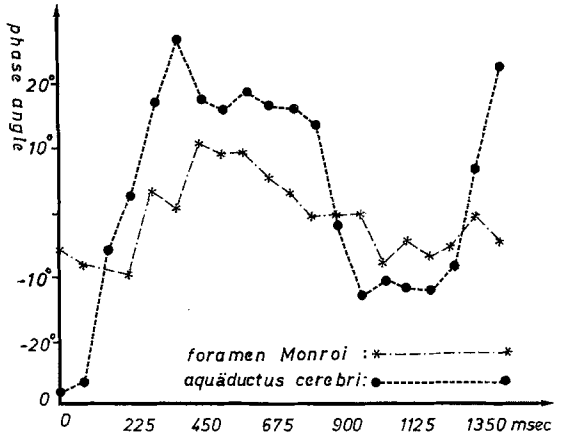

Fig. 7. Plot of the phase of the protons in the cerebral aqueduct and the interventricular foramen as a function of R wave delay

(Fig. 5). However, the signal from the adjacent superior cerebellar vein indicates constant blood flow directed upwards, as indicated by its black appearance in phase images. Comparison of magnitude and phase images indicates that in the cerebral aqueduct the change of phase of the CSF protons precedes the signal increase for about one or two images. This delay of 50–150 ms between signal strength and phase can be confirmed by the plot of the CSF voxels in the centre of the cerebral aqueduct when phase and intensity are presented in the same diagram (Fig. 6). The signal increase following the CSF oscillation from the third to the fourth ventricle is greater than the second increase of signal intensity, which follows the backflow from the fourth to the third ventricle.

Analysis of phase and signal change of the CSF protons in the cerebral aqueduct indicates that CSF flow from the third to the fourth ventricle normally starts 200 ms after the R wave of the ECG and simulates an arterial pulse pattern with an early systolic peak, followed by a shoulder. This downward flow lasts for 55–60 % of the cardiac cycle and is followed by backflow from the fourth to the third ventricle in the last third and the first 100 ms of the cardiac cycle. A similar pattern of CSF flow was detectable in the outlet foramina of the fourth ventricle.

ECG-gated sequences perpendicular to the foramen of Monro, through the third or lateral ventricles, and through the foramen itself, failed to demonstrate reproducible signal increase during the cardiac cycle. Analysis of the proton phase, however, revealed a short, early systolic backflow from the third to the lateral ventricles followed by slow CSF motion from the lateral to the third ventricle (Fig. 7). Amplitude, velocities, and volume of the oscillating CSF flow through for foramen of Monro were too small to result in a significant, reproducible signal increase and were detectable by analysis of the proton phase only.

In contrast to the two peaks of signal intensity in the cerebral aqueduct, only one signal increase was detectable in the anterior and lateral cervical subarachnoid space during one cardiac cycle (Fig. 8 a). Figure 9 a shows the asynchronously different patterns of CSF flow: maximal signal intensities were detectable in the lateral subarachnoid space during the early phase of the cardiac cycle, and anteriorly 300 ms later. The phase image (Fig. 9 b), however, demonstrates synchronous downward oscillating motion of the CSF in both compartments during cardiac systole, followed by a diastolic backflow with a negative shift laterally and a positive shift anteriorly, which indicates additional upward flow in the former site and downward flow in the latter. If the velocity of the bulk flow was equal to or greater than the oscillating motion (which was the case in most of our investigations) no signal increase was detectable on the magnitude images when the two moved in opposite directions. However, the resulting intensity peak was increased when oscillating and directed flow moved in the same direction.

Additional saturation pulses were used to confirm these results (Fig. 10). After saturation of a plane cranial to the slice examined, the signal peak resulting from downward flow anteriorly was reduced (Fig. 8 b). In contrast, the lateral signal increase disappeared after saturation of a slice below (Fig. 10). Thus, in the cervical canal, the cardiac-related oscillating motion of the CSF was superimposed upon additional bulk flow moving in separate channels, mainly directed downwards in the anterior and upwards in the lateral compartments of the subarachnoid space.

Comparison of the phase diagrams of the CSF protons in the cerebral aqueduct (Fig. 6) and the cervical subarachnoid space (Fig. 9 b) revealed that cervical systolic CSF downward flow precedes aqueduct flow by about 50–100 ms; this finding was confirmed using a field-even echo rephasing sequence [12] (Fig. 11).

Discussion

Since Du Boulay's investigations [3, 4], there is no longer any doubt that the oscillating CSF pulsation is a response to the transient increase of intracranial blood volume during the cardiac cycle. The arterial inflow of blood has an early systolic peak about 100 ms after the R wave of the

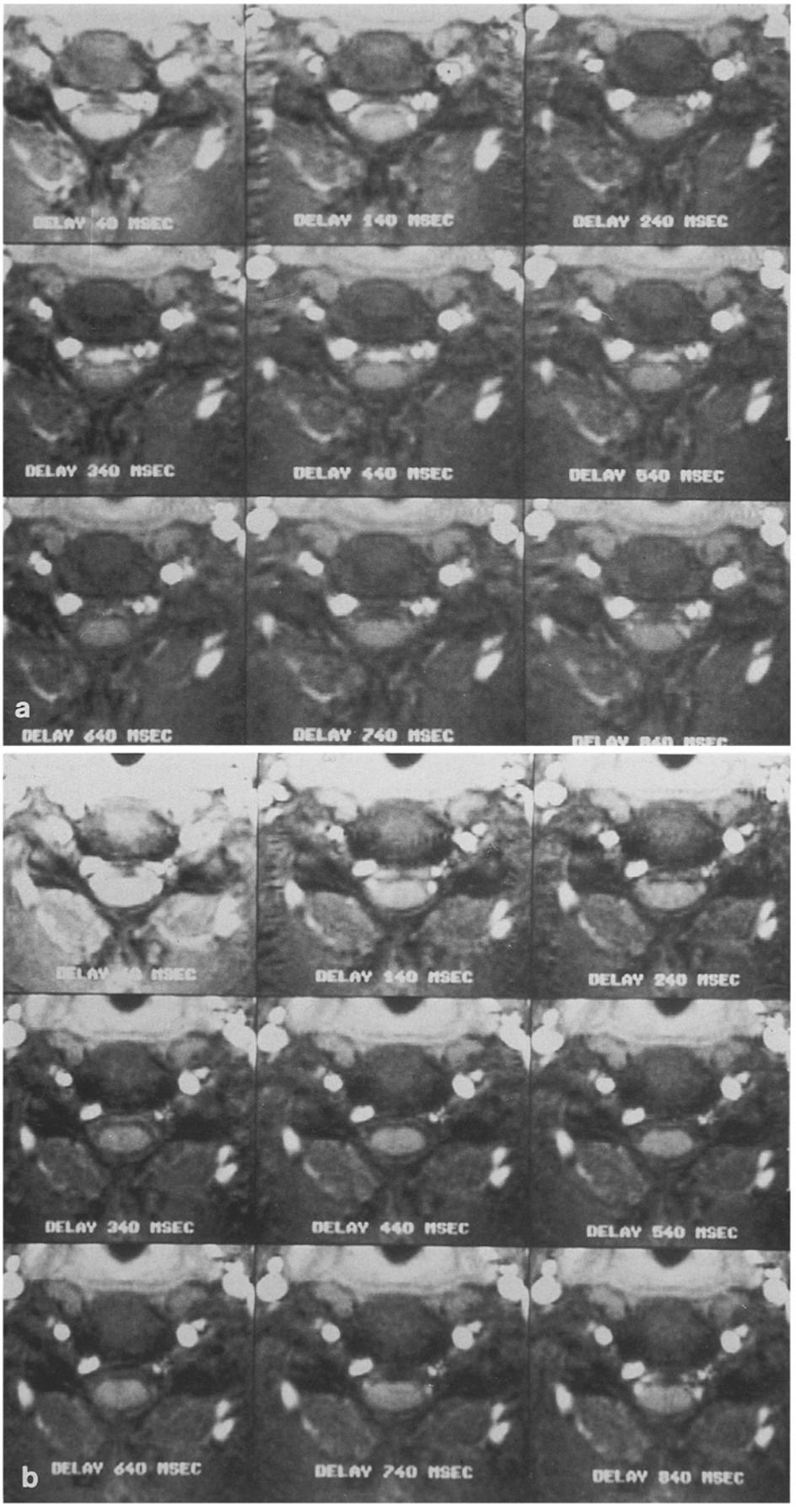

Fig. 8. Signal intensities in the cervical spinal canal during the cardiac cycle without (**a**) application of an additional saturation pulse (**b**). After presaturation of a plane cranial to the slice examined, the signal increase in the anterior subarachnoid space 300–400 ms after the R wave of the ECG is diminished (**b**)

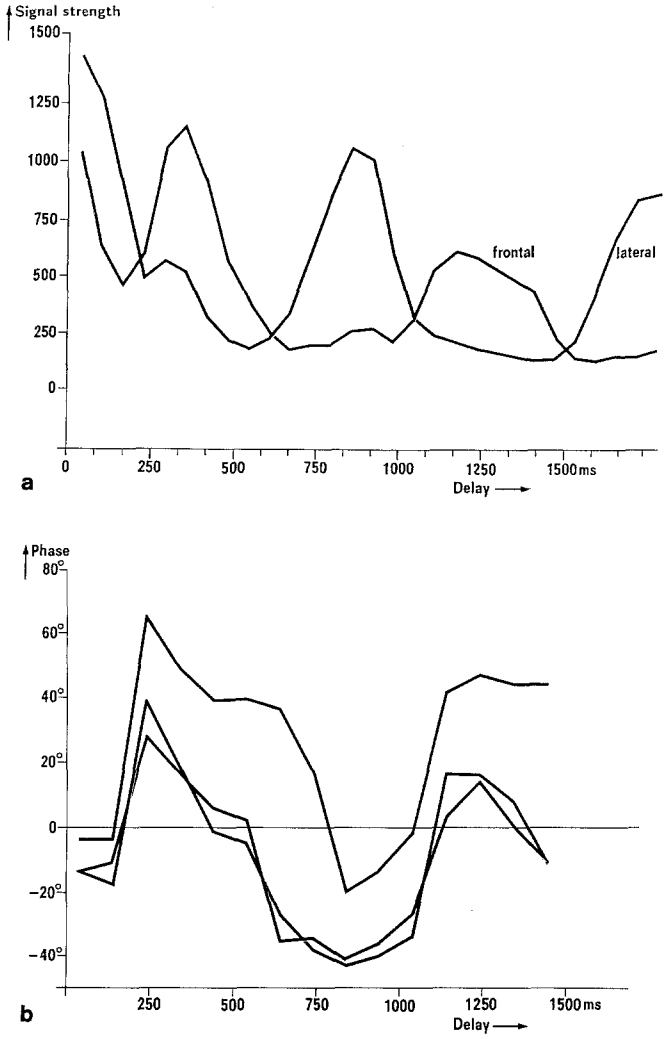

Fig. 9. Plot of signal intensities (**a**) and phase (**b**) of CSF in the anterior and lateral cervical subarachnoid space as a function of R wave delay of the ECG. The phase of the protons in the anterior subarachnoid space is shifted to positive values, indicating superimposed continous flow upwards, whereas the CSF in the lateral CSF channels demonstrates negative phase shift

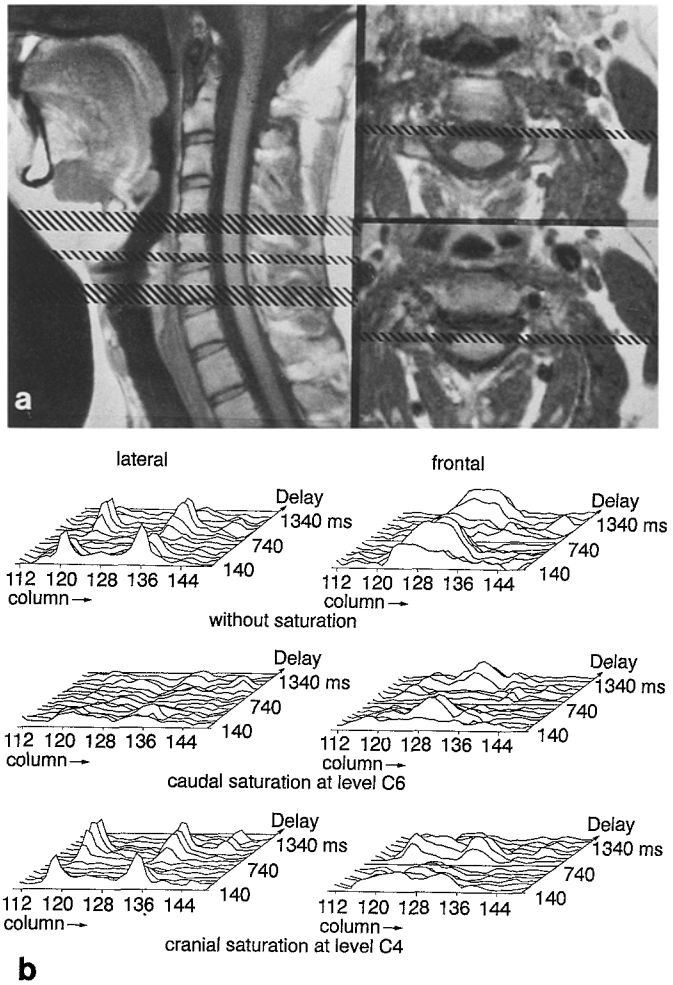

Fig. 10 a, b. 3-D diagram of the cardiac-related CSF motion in the cervical spinal canal at the level of the fifth cervical vertebra. **a** The localization of the presaturation slices above and below the plane examined is shown on the sagittal T1-weighted image. The columns through the lateral and anterior subarachnoid space are marked on axial images. **b** The oscillating CSF signal increase during the cardiac cycle in the lateral/anterior cervical spinal channels is diminished after presaturation of slices below/above the plane investigated

ECG (Fig. 12 a); in contrast, venous outflow is almost continuous (Fig. 12 b), with only a subtle diastolic flow increase in the internal jugular vein. This results in a transitory systolic increase in blood volume inside the indistensible skull, which must be compensated for by displacement of CSF.

Our results show that systolic expansion of the arteries of the circle of Willis cannot be the cause of CSF pulsation. Comparison of the periodic course of phase and magnitude of the blood protons in the carotid and vertebral arteries (Fig. 12) and of the CSF protons in the cervical spinal canal (Fig. 9) and cerebral aqueduct (Fig. 6) revealed that there is a delay of about 100–200 ms between the arterial pulse wave and the downward flow of CSF in the cervical spinal canal and the cerebral aqueduct, respectively. Moreover, during cardiac systole CSF motion in the fourth ventricle and the aqueduct is directed downwards, and not away from the arteries of the circle of Willis.

It was suggested by Bering [13] and Gardner [14] that CSF pulsation is generated by systolic expansion of the choroid plexus. Since the greatest part of the choroid plexus is inside the lateral ventricles, marked CSF flow from the lateral to the third ventricle should be expected during cardiac systole. On the other hand, the notion of a CSF pump in the third ventricle, consisting of systolic cardiac-related rhythmic squeezing between the two thalami, proposed by O'Connell [15], requires marked CSF backflow from the third to the lateral ventricle during systole.

Using ECG-gated magnitude images, signal increase in the foramen of Monro was detectable in only a few subjects. Moreover, these increases were seen inconstantly, most often during late systole, even when highly sensitive ECG-gated FLASH sequences with a slice thickness of 2 mm were used. Analysis of the proton phase, however, revealed a very short initial retrograde CSF flow at the foramen of Monro from the third to the lateral ventricle, followed by late systolic downward flow in the same direc-

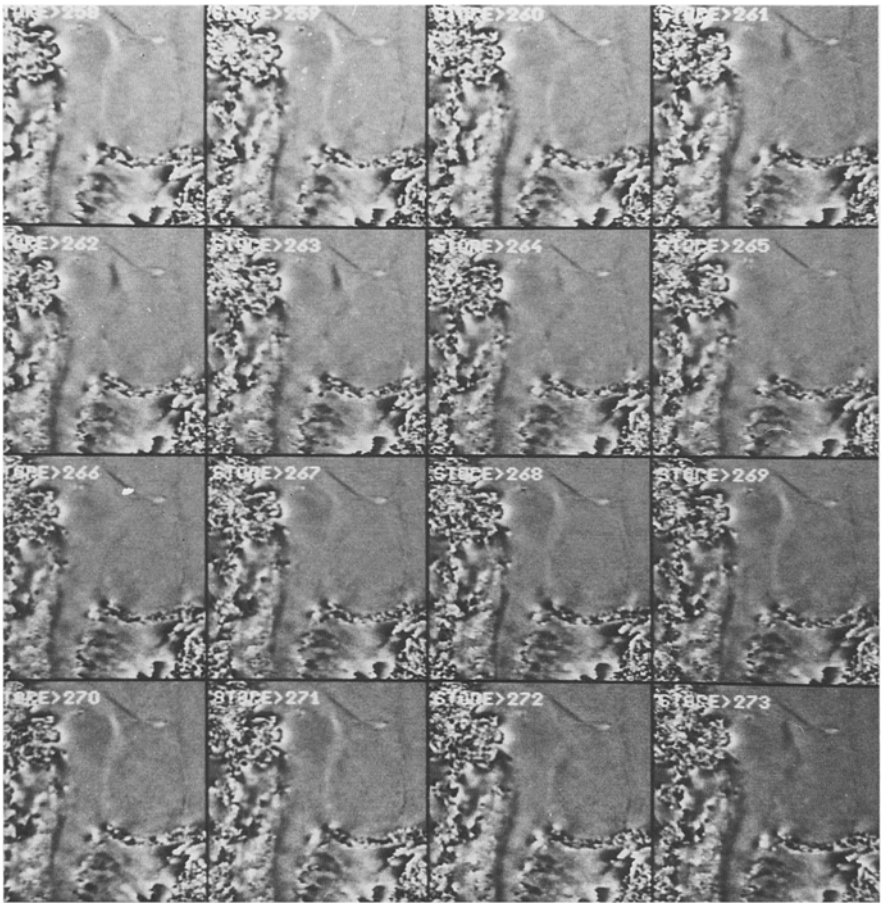

Fig. 11. ECG-gated midsagittal field even-echo rephasing sequence (75 ms/15 ms/60°; flow upwards encoded as signal increase, downwards as signal decrease). The image 150 ms after the R wave of the ECG (store 260) clearly demonstrates systolic flow acceleration downwards in the anterior cervical subarachnoid space, whereas flow in the cerebral aqueduct is still upwards

tion as in the cerebral aqueduct (Fig. 7). Amplitude and velocities of CSF motion through the foramen of Monro, as detected by analysis of the proton phase, were too low to result in a reliable and reproducible signal increase on the magnitude images.

In accordance with the findings of Du Boulay [4] and of Lane and Kricheff [5], analysis of the change of signal intensities and phase of the CSF protons indicates that amplitudes, velocities, and volumetric displacement of CSF pulsation are maximal in the cervical spinal canal. Moreover, this cardiac generated oscillating CSF motion is superimposed on additional bulk flow moving in separate subarachnoid channels [9]. Using our flow phantom (Fig. 4), a similar flow pattern could be obtained with continuous flow of about 20 mm/s through the tube fixed to the wagon; the wagon was then simultaneously moved forward and backward – "ECG gated" – with a frequency of 1 Hz and amplitudes of about 10–20 mm, resulting in maximum velocities of up to 50 mm/s. Thus, the CSF flow velocities obtained by MRI as calculated by computer simulation and flow phantom measurements were high when compared to those given by invasive techniques [5] with installation of air or positive contrast medium into the subarachnoid space.

Our results support Du Boulay's conclusion [3] that the brain is the most important CSF pump. He suggested that the increased blood volume forced into the brain during cardiac systole causes the hemispheres to expand and to displace CSF downwards into the spinal canal, and that this is possible because of the elasticity of its walls, due mainly to the large epidural veins with free extraspinal connections. Due to the restricted technical possibilities at that time, Du Boulay found no CSF motion through the foramen of Monro and concluded that the pressure in and around the supratentorial ventricles normally rises simultaneously and to the same degree.

Comparative MRI analysis of signal intensity and the proton phase in different CSF compartments leads to the conclusion that the cardiac-related pulsatile CSF flow begins with rapid, early systolic displacement of a relatively large volume of CSF from the intracranial subarachnoid space into the cervical spinal canal. This downward flow precedes the CSF motion inside the ventricles by about 50–100 ms. Thus, considering the time course of CSF flow and the volume of pulsatile CSF displacement, it is obvious that the flow in the cervical spinal canal cannot be the result of the pulsatile ventricular CSF motion.

Considering the brain as the main pump for the circulation of the CSF, we can assume that the increased systolic intracranial blood volume accumulates mainly in the richly vascularized compartments of the brain. Therefore, it is not surprising to find that a large volume of CSF is initially displaced from the subarachnoid space adjacent to the richly vascularized grey matter into the cervical spinal canal immediately after the inflow of systolic blood. Moreover, computerized volumetric MRI measurements

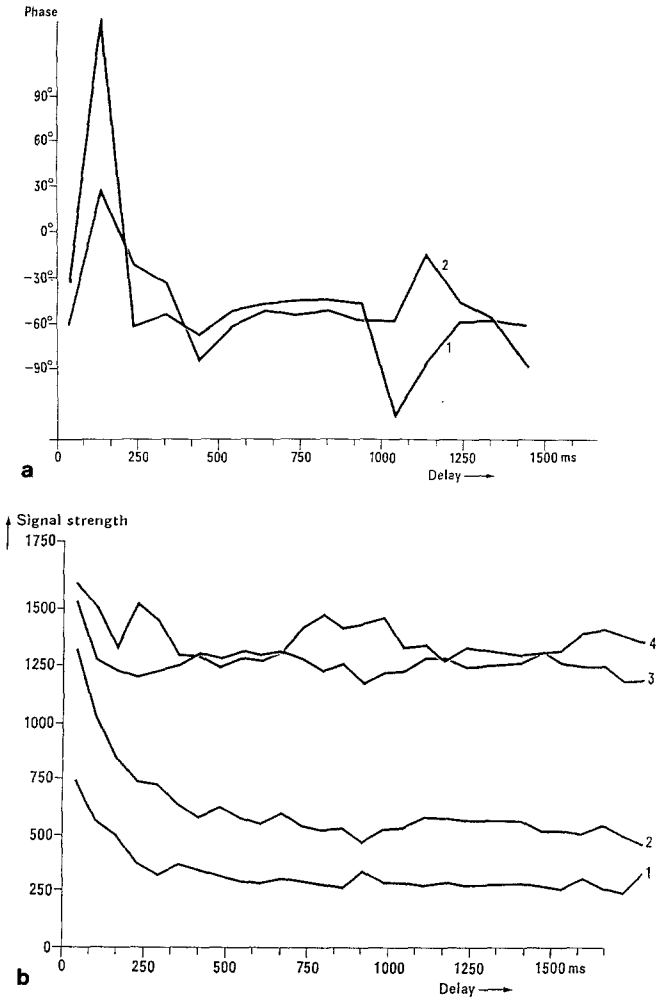

Fig. 12. Diagrams of phase (**a**) and signal strength (**b**) measured in an axial plane through the C3 vertebral body demonstrate flow acceleration in the internal carotid and vertebral arteries (*1, 2* in **a**) during early systole in contrast to the almost continous blood flow in the epidural *(4)* and internal jugular veins *(3)*, which shows a subtle, typically double – peaked, diastolic flow increase. Signal intensity of muscle tissue *(1)* and the spinal cord *(2)* is decreased due to saturation effects (FLASH/75 ms/10 ms/90°)

of the intracranial CSF spaces confirm that the ventricular volume is only 10–20% of that of the intracranial subarachnoid CSF compartment [16].

CSF flow inside the ventricular system was found to begin about 50–100 ms later than the early systolic displacement of CSF from the intracranial subarachnoid space into the cervical spinal canal following the distension of the grey matter of the hemispheres. In the ventricular system, CSF is initially forced from the third ventricle down the aqueduct and out of the fourth ventricle. At the same time there is a very short backflow through the foramen of Monro, resulting in displacement of a minute volume of CSF from the third to the lateral ventricles, detectable only by analysis of the proton phase (Fig. 7). Thus, the pressure inside the ventricular system rises primarily in the third ventricle, where for a few milliseconds it is higher than that in the lateral ventricles. A few milliseconds later, however, there is very subtle systolic downward flow of CSF through the foramen of Monro from the lateral to the third ventricle. This movement, and the initial systolic backflow, are easily detected by analysis of the proton phase. However, significant flow-induced signal increase is seldom detectable on the corresponding magnitude images in the interventricular foramen. As shown above (Fig. 3), this constellation of phase and signal strength confirms that there is very small amplitude oscillation of CSF through the interventricular foramen; thus the same and therefore presaturated protons are moved through the slice examined.

Comparative analysis of phase and signal strength of protons in different CSF compartments indicates that cardiac-related CSF pulsation begins with an early systolic compression of the intracranial subarachnoid space surrounding the cerebral hemispheres, due to expansion of the grey matter. Secondly, the third ventricle is sequeezed by increased systolic blood flow into the thalamus and basal ganglia. This results in flow of CSF down the aqueduct and out of the fourth ventricle, and brief backflow from the third to the lateral ventricles, followed by a subtle outflow from the lateral to the third ventricle.

However, to obtain one sequence of FLASH images, 256 ECG-gated gradient echo measurements must be made, as has been shown above. Our results thus demonstrate the average CSF pulsation during 256 cardiac cycles, whereas other effects of CSF flow are lost. To reveal these, especially the respiration-related components of the CSF flow, other MRI techniques must be used [17, 18].

References

1. Di Chiro G (1964) Movement of the cerebrospinal fluid in human beings. Nature 204: 290–291
2. Di Chiro G (1966) Observations on the circulation of the cerebrospinal fluid. Acta Radiol 5: 988–1002
3. Du Boulay GH (1966) Pulsatile movements in the CSF pathways. Br J Radiol 39: 255–262
4. Du Boulay GH, O'Connell J, Currie J, Bostick T, Verity P (1972) Further investigations on pulsatile movements in the cerebrospinal fluid pathways. Acta Radiol 13: 496–523
5. Lane B, Kricheff II (1974) Cerebrospinal fluid pulsations at myelography: a videodensitometric study. Radiology 110: 579–587
6. Bergstrand G, Bergström M, Nordell B, Stahlberg F, Ericsson A, Hemmingson A, Sperber G, Thuomas KA, Jung B (1985) Cardiac gated MR imaging of cerebrospinal fluid flow. J Comput Assist Tomogr 9: 1003–1006
7. Edelman RR, Wedeen VJ, Davis KR, Widder D, Hahn P, Shoukimas G, Brady TJ (1986) Multiphasic MR imaging: a new method for direct imaging of pulsatile CSF flow. Radiology 161: 779–783
8. Feinberg DA, Marks AS (1987) Human brain motion and cerebrospinal fluid circulation demonstrated with MR velocity imaging. Radiology 163: 793–799
9. Schroth G, Klose U, Gawehn J, Petersen D, Varallay G (1987) ECG-related pulsations of the CSF. Society of Magnetic Resonance in Medicine, 6th Annual Meeting, New York, Book of Abstracts, p 119
10. Sherman JL, Citrin CM (1986) Magnetic resonance demonstration of normal CSF flow. AJNR 7: 3–6
11. Haase A, Frahm J, Matthaei D, Hänicke W, Merboldt KD (1986) FLASH Imaging. Rapid NMR imaging using low flip-angle pulses. J Magn Reson 67: 258–266

12. Firmin DN, Nayler GL, Klipstein RH, Underwood SR, Rees RSO, Longmore DB (1987) In vivo validation of MR velocity imaging. J Comput Assist Tomogr 11: 751–756
13. Bering AE (1962) Circulation of cerebro-spinal fluid. Demonstration of the chorioid plexus as the generator of the force for flow of fluid and ventricular enlargement. J Neurosurg 19: 405–412
14. Gardner WJ (1965) Hydrodynamic mechanism of syringomyelia. Its relationship to myelocele. J Neurol Neurosurg Psychiatry 28: 247–259
15. O'Connell JEA (1943) Vascular factor in intracranial pressure and maintenance of cerebro-spinal fluid circulation. Brain 66: 204–225
16. Schroth G, Naegele T, Klose U, Mann K, Petersen D (1988) Reversible brain shrinking in abstinent alcoholics measured by MRI. Neuroradiology 30: 385–389
17. Klose U, Schroth G, Müller E, Grodd W (1988) Echtzeit-Darstellungsmöglichkeiten von Liquorbewegungen in der Kernspintomographie. In: Nüsslin F (ed) Medizinische Physik – Deutsche Gesellschaft für Medizinische Physik, Tübingen, pp 562–566
18. Mueller E, Laub G, Graumann R, Loeffler W (1988) RACE – real time acquisition and evaluation of pulsatile blood flow on a whole body MRI unit. Society of Magnetic Resonance in Medicine, 7th Annual Meeting, San Franzisco, Book of Abstracts, vol. 1, p 729

Prof. G. Schroth
Department of Neuroradiology
Eberhard-Karls-Universität
Hoppe-Seyler-Strasse 3
W-7400 Tübingen
Federal Republic of Germany